Journal of Superconductivity and Novel Magnetism (2020) 33:1611–1617
https://doi.org/10.1007/s10948-019-05192-8

ORIGINAL PAPER

Effect of Magnesium Substitution on Structural and Magnetic Properties of Nickel Ferrite Nanoparticles

C. N. Anumol[1] · M. Chithra[1] · Shantinarayan Rout[2] · Subasa C. Sahoo[1]

Received: 30 January 2019 / Accepted: 17 June 2019 / Published online: 26 June 2019

Abstract

Magnesium-substituted Ni-ferrite ($Mg_xNi_{1-x}Fe_2O_4$; $0 \le x \le 1$) nanoparticles were prepared by sol-gel method and were annealed at 550 °C and 900 °C in air. All the as-prepared samples and the samples annealed at 550 °C were single phase whereas some additional peaks of α-Fe_2O_3 was observed for the samples annealed at 900 °C. Lattice constant increased with the increase in Mg^{2+} concentration. Crystallite size did not show any systematic variation with the increase in Mg^{2+} concentration and was increased after annealing in these nanoparticle samples. The highest M_S values of 42 and 46 emu/g were observed at 300 and 60 K respectively for the as-prepared sample with $x = 0.05$ and the lowest values of 21 and 26 emu/g were observed at 300 and 60 K respectively for the 550 °C-annealed sample with $x = 1$. The magnetization and coercivity decreased with the increase in Mg^{2+} concentration. The non-saturation behavior was found to be increased with the increase in Mg^{2+} concentration in these samples. The observed magnetic behavior can be understood on the basis of increase in nonmagnetic Mg^{2+} concentration, cation distribution in the lattice sites, growth of crystallite size, and the decrease in anisotropy with the increase in Mg^{2+} concentration in these nanoparticle samples.

Keywords Ferrite · Nanoparticles · Substitution · Annealing · Magnetic properties

1 Introduction

Ni-ferrites ($NiFe_2O_4$) with several interesting properties like moderate saturation magnetization, low coercivity, low electrical losses, high electrical resistivity, and good chemical stability find many applications in technology, environmental, and biomedical fields [1, 2]. Ni-ferrite has inverse spinel structure with 8 Fe^{3+} in the tetrahedral A-sites and the rest 8 Fe^{3+} together with 8 Ni^{2+} in the octahedral B-sites in the unit cell [3]. When these ferrites are prepared in nanoscale, its physical properties are modified due to smaller crystallite sizes and their distribution in the nanomaterial samples. The magnetic properties of these ferrites can also be modified by substituting different cations and site occupancy of these cations in the spinel structure. Mg^{2+} is a nonmagnetic ion with no unpaired electron and prefers to occupy the B-site in the spinel structure. So, the substitution of Mg^{2+} in place of Ni^{2+} is expected to modify the super-exchange interaction and the physical properties of Ni-ferrite [4–6].

Substitution of Mg^{2+} has been reported to modify the electrical, optical, electrochemical, and photocatalytic properties of Ni-ferrite nanoparticles. Hirthna et al. reported the decrease in dielectric properties and increase in electrical conductivity with increasing Mg^{2+} concentration in $Mg_xNi_{1-x}Fe_2O_4$ nanoparticles [4]. The dielectric properties of $Mg_xNi_{1-x}Fe_2O_4$ nanoparticles have also been studied by many other researchers [7–9]. Shobana et al. suggested from their electrochemical study that Mg^{2+} substituted Ni-ferrite nanoparticles can be used as anode material for rechargeable batteries [10]. Nadumane et al. studied that Mg^{2+} substituted Ni-ferrite nanoparticles show better photocatalytic properties than the Ni-ferrite nanoparticles [11]. In the present work, we studied the effect of Mg^{2+} concentration and annealing temperature on the magnetic behavior of $Mg_xNi_{1-x}Fe_2O_4$ nanoparticles prepared by sol-gel method.

Electronic supplementary material The online version of this article (https://doi.org/10.1007/s10948-019-05192-8) contains supplementary material, which is available to authorized users.

✉ Subasa C. Sahoo
subasa.cs@gmail.com

[1] Department of Physics, Central University of Kerala, Kasaragod, Kerala 671316, India

[2] Department of Physics, Ravenshaw University, Cuttack, Odisha 753003, India

2 Experiments

Magnesium-substituted nickel ferrite ($Mg_xNi_{1-x}Fe_2O_4$; $0 \leq x \leq 1$) nanoparticles were synthesized by sol-gel autocombustion method. Metal nitrates of nickel and magnesium were used as the starting salts, and ethylene glycol was used as solvent. The detailed synthesis method has been reported elsewhere [12]. After auto-combustion, the powders were collected at room temperature. The powders were ground well using agate mortar pestle and were subsequently annealed at 550 °C and 900 °C in air for 2 h. Structural properties were studied by a Rigaku Miniflex 600 X-ray diffractometer with Cu-Kα radiation ($\lambda = 1.5406$ Å) in θ/2θ mode. Microstructural studies were carried out using Carl Zeiss Sigma field emission gun scanning electron microscope (FEG-SEM). Magnetic properties were studied by a vibrating sample magnetometer (VSM) of Quantum Design Versa Lab Physical Property Measurement System by applying maximum magnetic field up to ± 30 kOe at different temperatures.

3 Results and Discussion

3.1 Structural and Microstructural Properties

Figure 1 shows the X-ray diffraction patterns of the as-prepared (asp) and the samples annealed at 900 °C. All the observed peaks were indexed with the help of standard JCPDS data of Ni-ferrite (PDF card No. 742081) and Mg-ferrite (PDF Card No.732410). As seen in Fig. 1a, all the asp samples were of single phase, whereas for the samples annealed at T_A = 900 °C with $x \leq 0.25$, one peak corresponding to α-Fe_2O_3 was observed in addition to the Ni-ferrite phase as seen in the Fig. 1b. Lattice constant increased with the increase in Mg^{2+} concentration in both the asp and annealed samples and was found to be in the range of 8.309 to 8.456 Å for these nanoparticle samples compared to the standard value of 8.337 Å and 8.376 Å for Ni-ferrite and Mg-ferrite respectively. Crystallite size of these nanoparticle samples was calculated by Scherrer's formula using the most intense peak [13]. It did not show any systematic variation with the increase in Mg^{2+} concentration and was found to be 16 ± 2, 19 ± 4, and 38 ± 9 nm for the asp, 550 °C, and 900 °C-annealed samples respectively.

Figure 2a, b, c, d show the FEG-SEM images with different magnifications of the asp and annealed (T_A = 900 °C) $Mg_xNi_{1-x}Fe_2O_4$ nanoparticle samples with $x = 0.85$. As seen in Fig. 2a, c, the crystallite size of the asp sample is very small. After annealing, bigger crystallites were observed (see Fig. 2b, d) in the sample. This observation corroborates our XRD observation about the growth of crystallites after annealing.

3.2 Magnetic Properties

Magnetic hysteresis (M-H) loops of the asp and annealed (T_A = 900 °C) $Mg_xNi_{1-x}Fe_2O_4$ nanoparticle samples with $x = 0.05$, 0.50, 0.85 are shown in Fig. 3. As seen in Fig. 3, the loops did not saturate up to the highest magnetic field of 30 kOe. Moreover, one can see that the loops of the annealed samples are better saturated than the asp samples. The magnetization values of all the samples were obtained by extrapolating the M-H loop at high field to the zero applied fields. The spontaneous magnetization (M_S) and coercivity (H_C) values obtained from the M-H loops are shown with the increase in Mg^{2+} concentration in Fig. 4. For the asp sample with $x = 0$, i.e., for Ni-ferrite sample, the M_S values of 38 and 42 emu/g were observed at 300 and 60 K respectively. As seen in Fig. 4a, b, for the asp and 550 °C-annealed samples, the M_S value slightly increases for $x = 0.05$ than that for $x = 0$; then it decreases with further increase in Mg^{2+}

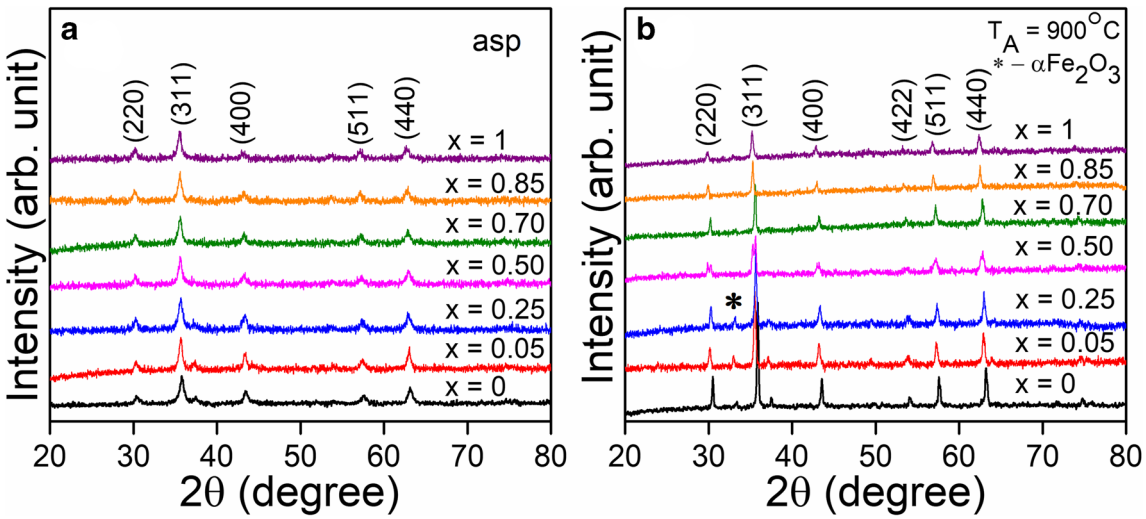

Fig. 1 XRD patterns of the **a** as prepared (asp) and **b** annealed (T_A = 900 °C) $Mg_xNi_{1-x}Fe_2O_4$ nanoparticle samples

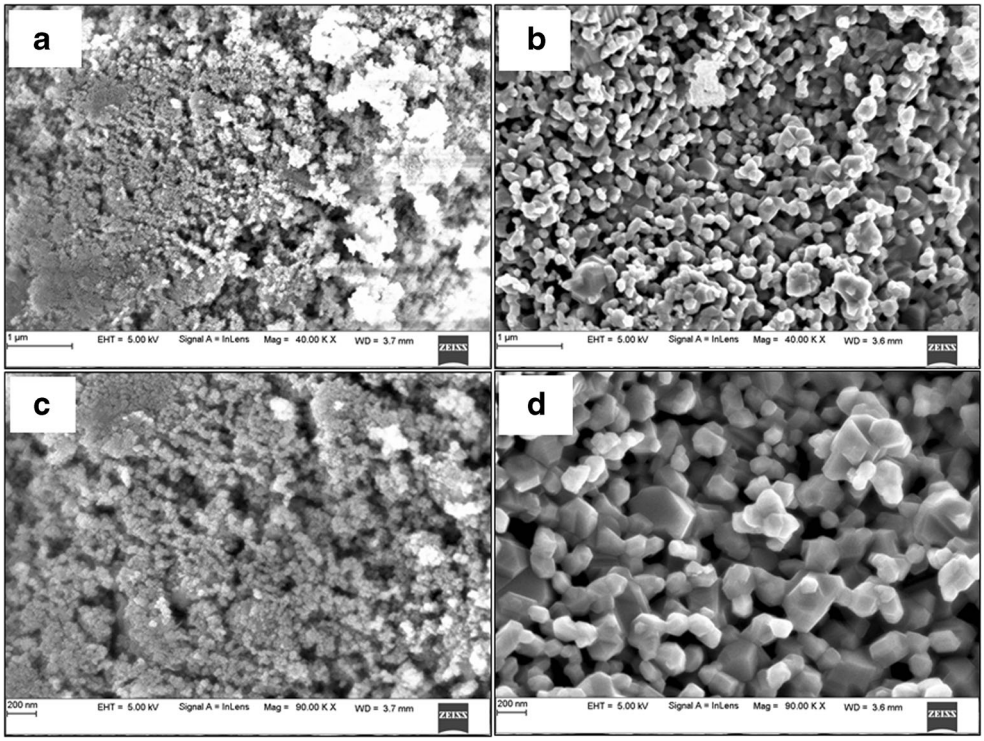

Fig. 2 FEG-SEM images of the **a** asp and **b** annealed ($T_A = 900$ °C) $Mg_{0.85}Ni_{0.15}Fe_2O_4$ nanoparticle samples. **c**, **d** The magnified images of the respective samples

concentration both at 300 K and 60 K. Hirthna et al. also observed increase in the M_S value up to $x = 0.6$ in $Mg_xNi_{1-x}Fe_2O_4$ nanoparticle samples [4]. However, many researchers reported monotonic decrease of M_S value with the increase in Mg^{2+} concentration [5, 6, 8]. Chavan et al. [5] observed the highest M_S of 64.5 emu/g at room temperature for $x = 0$, i.e., for Ni-ferrite nanoparticles. Naidu et al. [6] observed the maximum M_S value of 44.4 emu/g at 300 K for $x = 0$. Moradmard et al. [8] reported the maximum M_S value of 28.8 emu/g for $x = 0$ at room temperature. We observed the highest M_S values of 42 and 46 emu/g at 300 and 60 K respectively for $x = 0.05$. Moreover, the M_S value for the 550 °C-annealed samples is lower than that for the asp sample for all x values. For the samples annealed at 900 °C, M_S value

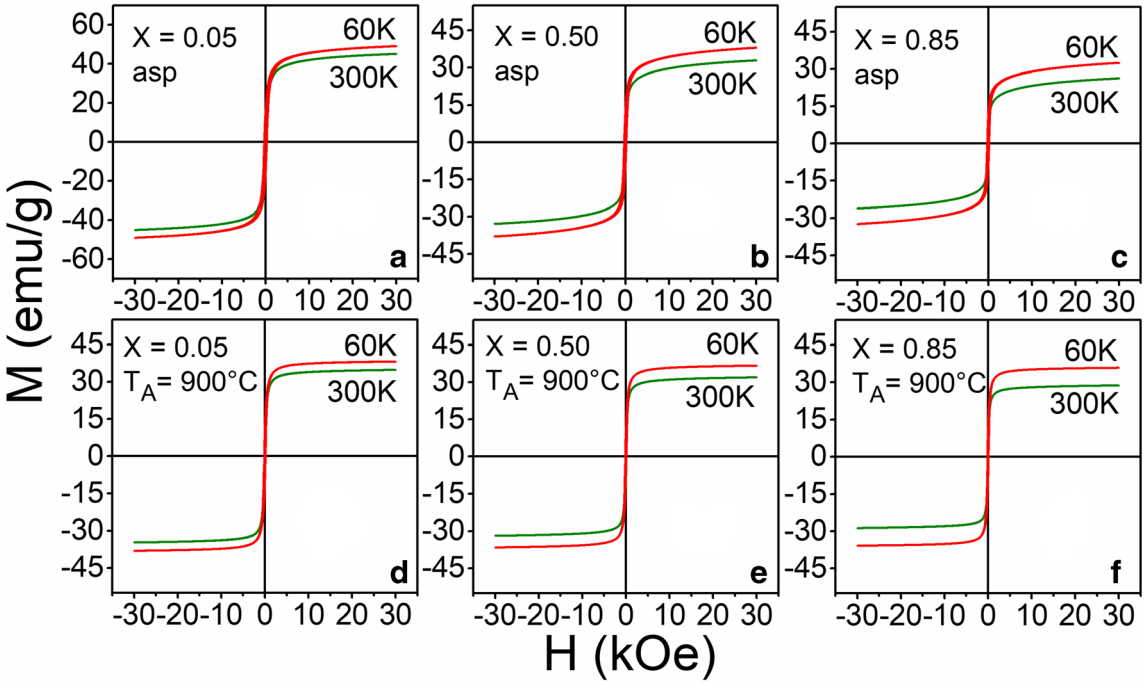

Fig. 3 M-H loops of the **a**–**c** asp and **d**–**f** annealed ($T_A = 900$ °C) $Mg_xNi_{1-x}Fe_2O_4$ nanoparticle samples

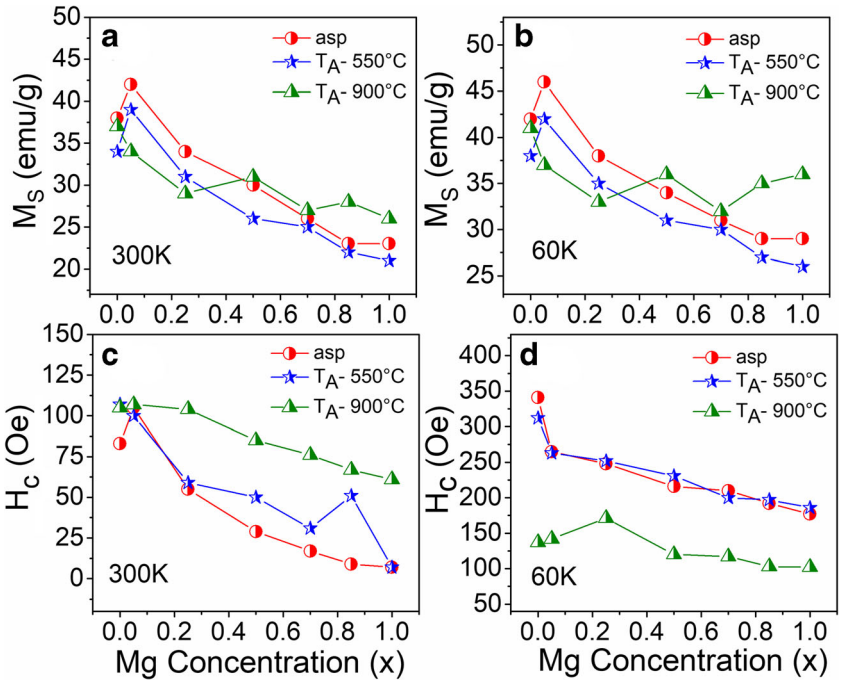

Fig. 4 Variation of M_S at **a** 300 K and **b** 60 K and H_C at **c** 300 K and **d** 60 K of $Mg_xNi_{1-x}Fe_2O_4$ nanoparticles with increase in Mg^{2+} concentration

continuously decreased from 37 emu/g observed for $x = 0$ to 29 emu/g for $x = 0.25$ at 300 K. With further increase in x value to 0.50, the M_S value slightly increased to 31 emu/g and then decreased with further increase in Mg^{2+} concentration. Similar trend was also observed at 60 K for the samples annealed at 900 °C. The lowest M_S values of 21 and 26 emu/g at 300 and 60 K respectively were observed for the sample annealed at 550 °C with $x = 1$, i.e., for Mg-ferrite. It is also seen in Fig. 4a, b that for $x = 0.05$ and 0.25, the M_S value monotonically decreased with increase in T_A. For higher Mg^{2+} concentration $x \geq 0.05$, the M_S value was the lowest for the sample annealed at $T_A = 550$ °C.

As seen in Fig. 4c, d, H_C decreased with the increase in Mg^{2+} concentration both at 300 K and 60 K. It is interesting to note that at 300 K, for the 900 °C-annealed samples, the H_C values were always the highest compared to those observed for the asp and 550 °C-annealed samples. However, at 60 K, though the H_C values were enhanced, it was the lowest for the 900 °C-annealed samples. The lowest H_C of ~10 Oe was observed at 300 K for the asp and 550 °C-annealed samples with $x = 1$, and the highest H_C of 340 Oe was observed at 60 K for the asp sample with $x = 0$.

The decrease in saturation magnetization with the increase in Mg^{2+} concentration in $Mg_xNi_{1-x}Fe_2O_4$ nanoparticles can be understood as follows. Ni^{2+} has two unpaired electrons in the valence shell and Mg^{2+} has no unpaired electron. Considering only spin contribution, Ni^{2+} has magnetic moment 2 μ_B and Mg^{2+} has 0 μ_B. As discussed earlier, both Mg^{2+} and Ni^{2+} prefer to occupy the B-site in the spinel structure. When Mg^{2+} ion is substituted into Ni-ferrite, it occupies B-site by replacing Ni^{2+} ion in the B-site and hence the effective magnetic moment in the B-site decreases. As a result, net magnetization decreases with the increase in Mg^{2+} concentration. The initial increase in magnetization for lower concentration of Mg^{2+}, i.e., for $x = 0.05$, may be due to the occupancy of some Mg^{2+} in the A-site [5, 14]. When some Mg^{2+} ions occupy the A-site and equal amount of Fe^{3+} ions are displaced to the B-site, the magnetization is higher in B-site compared to the A-site leading to increase in net magnetization value. As mentioned above, M_S value decreased with the increase in annealing temperature at 300 K for lower Mg^{2+}concentration, i.e., for $x = 0.05$ and 0.25. However, for higher Mg^{2+}concentration, i.e., for $x \geq 0.50$, M_S value initially decreases for $T_A = 550$ °C than that for asp sample and then increased with further increase in T_A to 900 °C. Similar trend was also observed at 60 K. With the increase in T_A, two factors control the magnetization in these nanoparticle samples. First one is that with the increase in crystallite size, volume contribution increases compared to the surface contribution in these nanoparticles which support enhancement in the magnetization with the increase in T_A. Another fact is that the Mg^{2+} ions present in the A-site moved to their preferred B-site with the increase in annealing temperature and crystallite size which results decrease in magnetization. As the crystallite size was not increased appreciably for the samples annealed at $T_A = 550$ °C, it can be understood that for $x = 0.05$ and 0.25, the migration of Mg^{2+} ions from A-site to the B-site results decrease in magnetization in these samples compared to the asp samples. For the samples annealed at $T_A = 900$ °C with $x \geq 0.50$, the crystallite growth is responsible for increase in magnetization. With the decrease in measurement temperature, the decrease in

thermal energy enhances the magnetization at lower temperature.

Coercivity in the nanomaterials is controlled by many factors like crystallite size, canting, magnetocrystalline, surface, and exchange anisotropies. Mg^{2+} has no anisotropy as it has zero orbital angular momentum (L) and zero spin angular momentum (S) compared to Ni^{2+} and Fe^{3+}. When Mg^{2+} concentration increases, magnetocrystalline anisotropy decreases in the sample. So, the H_C value decreases with the increase in Mg^{2+} concentration. The samples annealed at 900 °C contain α-Fe_2O_3 which is antiferromagnetic. Exchange anisotropy arises due to the interaction between the ferrimagnetic and antiferromagnetic grains in these samples. We believe that this exchange anisotropy in dominating in these samples leading to higher H_C at 300 K. Coercivity increases with the increase in single domain crystallite size up to the critical size and decreases with further increase in crystallite size due to the formation of multidomain. One can see that for the samples annealed at 900 °C, the H_C was not increased much at 60 K compared to the asp and 550 °C-annealed samples. The crystallite sizes are very small for the asp and 550 °C-annealed samples compared to the samples annealed at 900 °C. The surface anisotropy is dominating in these smaller crystallites compared to the bigger crystallites at low temperature [15]. Moreover, in the sample annealed at 900 °C, crystallite size is larger. With the increase in crystallite size, the surface anisotropy decreases. So, the H_C decreases with the increase in T_A at 60 K and the lowest value was observed for the samples annealed at 900 °C.

As mentioned earlier, the M-H loops were not saturated even at the highest applied field. So, for understanding the non-saturation behavior in detail, we used the method of law of approach to saturation [16]. We have fitted the initial curve of the M-H loop from 20 to 30 kOe to the equation

$$M(H) = M(\infty)\left[1-(H^*/H)^{1/2}\right] \quad (1)$$

where $M(\infty)$ is the magnetization at infinite applied field and H^* gives the information about non saturation related to the point like defects and anisotropy fluctuation at atomic level. Our experimental data was fitted well with this equation (see supplementary data). The variation of $M(\infty)$ and H^* values with the increase in Mg^{2+} concentration is shown in Fig. 5. It is seen from Figs. 5a and 5b that, $M(\infty)$ values slightly increased for lower concentration of Mg^{2+} ions (for $x = 0.05$) both at 300 and 60 K, and then it decreased with further increase in Mg^{2+} concentration as observed in the variation of M_S values shown in Fig. 4a, b. It is also observed in Fig. 5 that the $M(\infty)$ values of the asp samples were the highest and decreased with the increase in T_A for the sample with $x \leq 0.7$. The highest $M(\infty)$ values of 50 and 54 emu/g were observed for the asp sample with $x = 0.05$ at 300 K and 60 K respectively. For the asp samples and the samples annealed at 550 °C, H^* value initially decreases as the "x"value increases from 0 to 0.05 both at 300 K and 60 K as seen in Fig. 5c, d. For $x > 0.05$, there is an overall increase in H^* value with the increase in Mg^{2+} concentration. For the samples annealed at 900 °C, H* values were always the lowest both at 300 and 60 K. Moreover, the H^* values were almost constant with

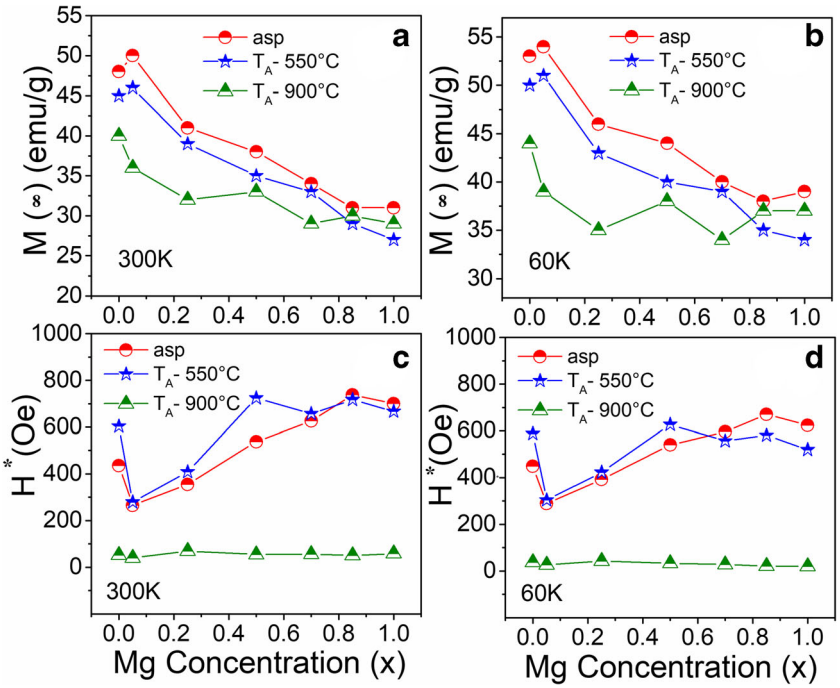

Fig. 5 Variation of $M(\infty)$ at **a** 300 K and **b** 60 K and H^* at **c** 300 K and **d** 60 K of $Mg_xNi_{1-x}Fe_2O_4$ nanoparticles with increase in Mg^{2+} concentration

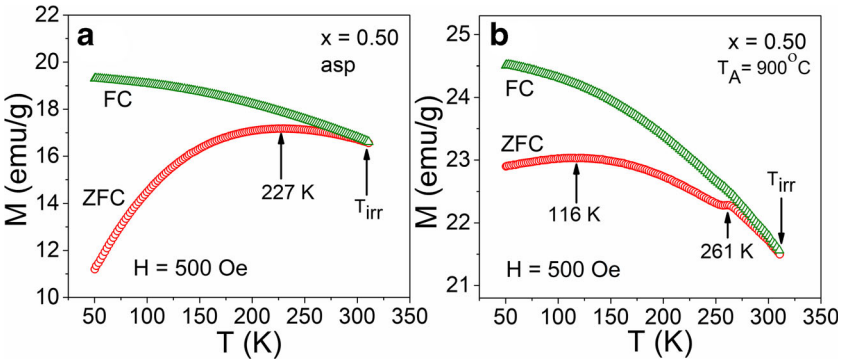

Fig. 6 Zero-field-cooled (ZFC) and field-cooled (FC) magnetization curves of the **a** asp and **b** annealed ($T_A = 900$ °C) $Mg_{0.50}Ni_{0.50}Fe_2O_4$ nanoparticle samples

increase in Mg^{2+} concentration both at 300 and 60 K for these samples.

The non-saturation in magnetic nanoparticles can be due to several factors like spin canting, cation distribution, presence of super-paramagnetic grains, and different anisotropies in the material [16]. As mentioned earlier for the asp samples and the samples annealed at 550 °C, M_S value slightly increased when "x" value increased from 0 to 0.05 and is due to the possible cation redistribution of Mg^{2+} and Fe^{3+} ions in the A- and B-sites. We also noticed that for the same samples, H^* value initially decreases as "x" value increased from 0 to 0.05. So, the initial decrease in the H^* value for the lower concentration of Mg^{2+} is due to the cation distribution in the spinel structure. With the increase in Mg^{2+} concentration $x > 0.05$, the increase in nonsaturation with increase in Mg^{2+} concentration for the asp samples, and the samples annealed at 550 °C may be due to the spin canting in the antiferromagnetically coupled lattice sites in the spinel structure. In these samples, the crystallite sizes are very small. So, the presence of super-paramagnetic grains in these samples also contributes to the non-saturation. As mentioned earlier, surface anisotropy plays significant role in smaller grains; it may also contribute to the non-saturation of magnetic moments and the increase in H^* in the asp samples and the samples annealed at 550 °C. The lowest H^* values were observed for the samples annealed at 900 °C, and there is not much change in the H^* values with the increase in Mg^{2+} concentration and with the decrease in temperature from 300 to 60 K. The decrease in surface defects and canting decreases the H^* values with the increase in crystallite size for the samples annealed at 900 °C.

Zero-field-cooled (ZFC) and field-cooled (FC) magnetization curves of the asp and annealed ($T_A = 900$ °C) samples with $x = 0.50$ are shown in Fig. 6. It is seen in Fig. 6 that the magnetization of FC curves of both asp and annealed samples decreases with the increase in temperature. As seen in Fig. 6a, a peak was observed around 227 K in ZFC curve for the asp sample. In the annealed sample, the peak was shifted to 116 K. A small kink was also observed around 261 K in this sample which may be due to the Morin transition of α-Fe_2O_3 present in the annealed samples [17, 18]. Both ZFC and FC curves meet, i.e., irreversible temperature (T_{irr}) was observed in both the asp and annealed samples around ~ 310 K.

4 Conclusion

$Mg_xNi_{1-x}Fe_2O_4$ nanoparticles were prepared by sol-gel method and were annealed at 550 °C and 900 °C in air. For the as-prepared samples and the samples annealed at 550 °C, the highest magnetization values were observed for Mg^{2+} concentration $x = 0.05$, and for samples annealed at 900 °C, there was an overall decrease in magnetization values with the increase in Mg^{2+} concentration. At 300 K, the highest magnetization value of 42 emu/g was observed for the as-prepared sample with $x = 0.05$, and the lowest value of 21 emu/g was observed for the sample annealed at 550 °C with $x = 1$. The coercivity decreased with the increase in Mg^{2+} concentration both at 300 K and 60 K. It was always the highest at 300 K and the lowest at 60 K for the samples annealed at 900 °C. Non-saturation of magnetization increased with the increase in Mg^{2+} concentration for the as-prepared samples, and the samples annealed at 550 °C with x values lie between 0.05 and 1, i.e., for $0.05 \le x \le 1$ where as it was almost constant for the samples annealed at 900 °C. Crystallite size, decrease in ionic magnetic moment, cation distribution in the spinel structure, decrease in anisotropy with the increase in Mg^{2+} concentration explain the observed magnetic behavior in these nanoparticle samples.

References

1. Jacob, J., Khadar, M.A.: J. Appl. Phys. **107**, 114310 (2010)
2. Azizi, A., Sadrnezhaad, S.K.: Ceram. Int. **36**, 2241 (2010)
3. Smit, J., Wijin, H.P.J.: Ferrites. Cleaver – Hume Press Ltd., London (1959)
4. Hirthna, Sendhilnathan, S.: Ceram. Int. **43**, 15477 (2017)
5. Chavan, P., Naik, L.R., Belavi, P.B., Chavan, G., Ramesha, C.K.: J. Electron. Mater. **46**, 188 (2017)

6. Naidu, K.C.B., Madhuri, W.: J. Magn. Magn. Mater. **420**, 109 (2016)
7. Varshney, D., Verma, K.: Mater. Chem. Phys. **140**, 412 (2013)
8. Moradmard, H., Farjami Shayesteh, S., Tohidi, P., Abbas, Z., Khaleghi, M.: J. Alloys Compd. **650**, 116 (2015)
9. Chavan, P., Naik, L.R.: Vaccum. **152**, 47 (2018)
10. Shobana, M.K., Kim, K., Kim, J.: Phys. E Low-Dimensional Syst. Nanostructures. **108**, 100 (2018)
11. Nadumane, A., Shetty, K., Anantharaju, K.S., Nagaswarupa, H.P., Rangappa, D., Vidya, Y.S., Nagabhushana, H., Prashantha, S.C.: J. Sci. Adv. Mater. Devices. **4**, 89 (2018)
12. Chithra, M., Anumol, C.N., Sahu, B., Sahoo, S.C.: J. Magn. Magn. Mater. **401**, 1 (2016)
13. Cullity, B.D., Graham, C.D., Introduction to magnetic materials, Second edi, A John wiley & sons (2009)
14. Ateia, E.E., El-Bassuony, A.A.H., Abdellatif, G., Mohamed, A.T.: Silicon. **10**, 1687 (2018)
15. Mozul, K.A., Ol, L.P., Sizova, Z.I., Bludov, A.N., Pashchenko, V.A., Baumer, V.N., Vashchenko, V.V.: Low Temp. Phys. **39**, 365 (2013)
16. Chithra, M., Anumol, C.N., Sahu, B., Sahoo, S.C.: J. Magn. Magn. Mater. **424**, 174 (2017)
17. Pastor, J.M., Pérez-Landazbal, J.I., Gmez-Polo, C., Recarte, V., Larumbe, S., Santamarta, R., Fernandes Silva, M., Gmez Pineda, E.A., Winkler Hechenleitner, A.A., Lima, M.K.: Appl. Phys. Lett. **100**, 063102 (2012)
18. Wang, J., Aguilar, V., Li, L., gen Li, F., zhong Wang, W., meng Zhao, G.: Nano Res. **8**, 1906 (2015)